OBSERVATIONAL STUDIES OF STELLAR ROTATION

J. Bouvier[1]

Abstract. This course reviews the rotational properties of non-degenerate stars as observed from the protostellar stage to the end of the main sequence. It includes an introduction to the various observational techniques used to measure stellar rotation. Angular momentum evolution models developed over the mass range from the substellar domain to high-mass stars are briefly discussed.

1 Introduction

The angular momentum content of a star at birth impacts on most of its subsequent evolution (e.g. Ekström et al. 2012). The star's instantaneous spin rate and/or on its rotational history plays a central role in various processes, such as dynamo-driven magnetic activity, mass outflows and galactic yields, surface chemical abundances, internal flows and overall structure, and it may as well influences the planetary formation and migration processes. It is therefore of prime importance to understand the origin and evolution of stellar angular momentum, indeed one of the most challenging issues of modern stellar physics. Conversely, the evolution of stellar spin rate is governed by fundamental processes operating in the stellar interior and at the interface between the star and its immediate surroundings. The measurement of stellar rotation at various evolutionary stages and over a wide mass range thus provides a powerful means to probe these processes.

In this introductory course, an overview of the rotational properties of stars and of angular momentum evolution models is provided. In Section 2, various techniques used to measure stellar rotation are described. In Section 3, the rotational properties of solar-type and low-mass stars are reviewed. Angular momentum evolution models developed for low-mass stars are discussed in Section 4. Finally, the rotational properties of intermediate-mass and massive stars are briefly outlined in Section 5.

---

[1] UJF-Grenoble 1 / CNRS-INSU, Institut de Planétologie et d'Astrophysique de Grenoble (IPAG) UMR 5274, Grenoble, F-38041, France

Rotation measurements : a summary

Technique	Spectroscopy	Photometry	Interferometry	Sismology
Quantity	**Vsini**, dV/dθ	**Prot**, **dProt/dθ**	Veq, inc, **P.A.**, (dV/dθ)	Prot, **Ω(r)**, (inc)
Accuracy	~10%	~0.1-10%	~10-30%(?)	?
Application	All stars	Spotted stars	Bright nearby stars	Bright stars
Limitations	Spectral resolution	Light curve duration and sampling	Fast rotators	Long-term continuous light curves
Instruments (e.g.)	ESO/HARPS, VLT/Flames	CCD mosaics; CoRot, Kepler	ESO/VLTI; GSU/ Chara	CoRot, Kepler
Only 1 star has it all (Veq, Prot, inc, P.A., dP/dθ, Ω(r)) : the Sun				

N.B. If **Vsini** is known from line profile broadening and **P$_{rot}$** from rotational modulation, then, with an estimate of R$_*$, the inclination of the rotational axis follows: **P/sini = 2πR$_*$/vsini**

Fig. 1. A summary of measurement techniques used to derive the rotational properties of non-degenerated stars.

2 Measurement techniques

Stellar rotation can be measured through a variety of techniques. I illustrate here some of the most commonly applied ones to measure the rotation rates of non-degenerated objects. The various techniques are summarized in Figure 1.

2.1 Spectroscopy

Capt. Abney (1877) was apparently the first to consider the effect rotation would have on a stellar spectrum. He suggested that Doppler broadening of the photospheric line profiles should occur, as the light from the rotating surface goes through the entrance slit of the spectrograph. For a star with a linear equatorial velocity V_{eq}, the spectral broadening of photospheric lines amounts to $\Delta\lambda_L = (\lambda/c) \cdot V_{eq} \cdot \sin i$, where i is the inclination angle between the line of sight and the rotation axis. A star seen pole-on (i=0) exhibits no Doppler broadening, while a direct measurement of V_{eq} is obtained for an equator-on star (i=90deg). The isorotation locus on the stellar disk, i.e., points of the stellar surface having the same projected velocity, follows vertical stripes parallel to the rotational axis, whose wavelength shift is given by $\Delta\lambda = (\lambda/c) \cdot V_{eq} \sin i \cdot cos(l) \cdot sin(L)$, where l and L are respectively the latitude and longitude of a point at the stellar surface.

The integrated line profile of a rotating star is the sum of the intrinsic line profiles of all points on the stellar disk affected by their respective Doppler shifts. To first order, it can be described as the convolution product of the intrinsic, non-rotating line profile with a "broadening" function given by (cf. Carroll 1933; Gray 1973):

$$G(\lambda) = \frac{2(1-\epsilon)[1-(\Delta\lambda/\Delta\lambda_L)^2]^{1/2} + \frac{1}{2}\pi\epsilon[1-(\Delta\lambda/\Delta\lambda_L)^2]}{\pi\Delta\lambda_L(1-\epsilon/3)}$$

where ϵ is the temperature- and wavelength-dependent limb-darkening coefficient. In the Fourier domain, the convolution product becomes an arithmethic product, and the Fourier transform of $G(\lambda)$ has the interesting property of having successive zeroes at frequencies inversely proportional to $v\sin i$ (e.g., Dravins et al. 1990), with the first zero occuring at $\nu_1 \simeq (2/3)(c/\lambda_o) \cdot (v\sin i)^{-1}$. Thus, even without the knowledge of the intrinsic line profile, the projected stellar velocity can be precisely derived from the location of the first and subsequent zeroes in the Fourier transform of the observed profile. This powerful technique has been most succesfully applied to fast rotators ($v\sin i \geq 30$ kms^{-1}) as their first zero occurs in the well-sampled, high S/N low frequency Fourier domain. The highest $v\sin i$ measured so far with this technique, ~ 600 kms^{-1}, was reported for an O-type star in the Large Magellanic Cloud (Dufton et al. 2011). For a few bright stars, the Fourier technique may even provide an estimate of surface latitudinal differential rotation (Gray 1977; Reiners & Schmitt 2002). In contrast, this method is not well suited to slowly rotating stars ($v\sin i \leq 20$ kms^{-1}) whose first zero is usually lost in the high frequency Fourier noise.

A more common method used to measure the rotation rate of slow rotators is the cross-correlation analysis. Instead of measuring the Doppler broadening of a single line profile, this method consists in cross-correlating the observed photospheric spectrum with either a template spectrum of a star of similar effective temperature and negliglible rotation (Tonry & Davies 1979) (alternatively, a non-rotating model spectrum can be used) or with a digital mask that let light go through predefined wavelength ranges corresponding to the location of major photospheric lines (Griffin 1967; Baranne et al. 1979). The result of either process is a cross-correlation profile or function (CCF) whose width is proportional to $v\sin i$ and whose signal-to-noise ratio has been greatly enhanced thanks to the inclusion of thousands of spectral lines in its computation. The relationship between the CCF width and $v\sin i$ has to be properly calibrated using stars with known rotation rates (Benz & Mayor 1981, 1984; Hartmann et al. 1986). Other applications of the cross-correlation technique include the derivation of accurate radial velocities (CCF peak location) and metallicity (CCF area).

More sophisticated spectroscopic techniques have also been used to measure rotation rates. The Doppler imaging technique (Vogt & Penrod 1983) and the related Zeeman-Doppler imaging technique (Semel 1989; Donati et al. 1997) both take advantage of the relationship existing between the location of a feature at the surface of a rotating star and its position within the line profile (Khokhlova

1976). As the star rotates, the signatures of stellar spots (or magnetic compo-
nents in polarized light) move across the line profile and their monitoring allows
the reconstruction of surface brightness and/or magnetic maps. The shape of
the line profiles is thus periodically modulated by surface inhomogeneities, and
the modulation period provides a direct measurement of the star's rotational pe-
riod. Furthermore, the latitudinal drift of spots on the stellar surface probes the
rotational period at different latitudes, thus yielding an estimate of differential ro-
tation at the stellar surface. Specifically, the quantity $\Delta\Omega$ is derived by assuming
a simplified solar-like differential rotation law of the form:

$$\Omega(\theta) = \Omega_{eq} - \Delta\Omega \sin^2 \theta \tag{2.1}$$

where Ω_{eq} is the angular velocity at the stellar equator and θ the latitude at the
stellar surface. The relationships between surface differential rotation on the one
hand and effective temperature, convective zone depth, and rotation rate on the
other, have been investigated for solar-type and lower mass stars by, e.g., Barnes
et al. (2005) and Marsden et al. (2011).

2.2 Interferometry

For relatively nearby stars, the stellar disk may be resolved by interferometry (e.g.
Kervella et al. 2004). In such a case, the stellar oblateness, i.e., the decimal part of
the ratio between the equatorial to the polar radii can be measured. For rapidly-
rotating stars, the stellar oblateness can be quite substantial. According to the
Roche model for stellar equipotential surfaces, the latitude-dependent radius of a
fast-rotating star is given by:

$$R(\omega, \theta) = \frac{3R_{pole}}{\omega \sin \theta} \cdot cos[\frac{\pi + cos^{-1}(\omega \sin \theta)}{3}]$$

where θ is the co-latitude and $\omega = \Omega/\Omega_{crit}$ is the ratio between the star's angular
velocity and the critical velocity at which centrifugal forces at the equator balance
gravity, $\Omega_{crit} = (\frac{2}{3})^{\frac{3}{2}} \cdot (\frac{GM}{R_p^3})^{\frac{1}{2}}$, where M is the stellar mass and R_p the polar radius,
Ekström et al. 2008). For a star rotating at critical velocity, the equatorial radius
is 1.5 times larger than the polar radius, yielding a stellar oblateness of 0.5. A
stellar oblateness with values up to 0.35 has been measured by interferometry for
a handful of massive stars rotating close to break-up velocity (cf. van Belle 2012).

Whenever interferometry can provide a fully reconstructed surface brightness
map for a rapidly rotating star, the gravity darkening effect can be directly ob-
served. von Zeipel (1924)'s theorem relates radiative flux to surface gravity and
thus predicts that a star rotating close to break-up will be brighter at the pole than
at the equator. This has actually been observed in Altair ($v \sin i$ =240 kms^{-1}) by
Monnier et al. (2007) who modeled the surface brightness map of this star to
derive both the inclination angle of the rotational axis on the line of sight and
its position angle on the sky plane. This illustrates the complementary power of
interferometry compared to spectroscopy, as the former delivers the orientation

of the angular momentum vector in space while the latter yields its (projected) modulus.

In fact, interferometry and spectroscopy can be combined, a technique called spectro-interferometry, to measure the position angle of the rotational axis of stars whose surface is not fully spatially resolved. The method consists in measuring the position of the star's photocenter across a spectral line. Each velocity channel within the line profile corresponds to one isorotation stripe at the stellar surface, parallel to the rotational axis. For instance, the far redward wing of the line profile spatially coincides with the limb of the receding hemisphere. As the photocenter is recorded across the line in successive velocity channels, its location slightly moves on the sky plane in a direction perpendicular to the rotational axis. Using several interferometric baselines with different orientations, the direction of the projected rotational axis can thus be derived. This challenging technique was successfully applied by Le Bouquin et al. (2009) to demonstrate that the position angle of Fomalhaut's rotational axis is perpendicular to the major axis of its planet-hosting debris disk.

2.3 Photometry

The oldest method used to measure stellar rotation consists in monitoring the visibility of magnetic spots on the stellar surface. In the Western world, Galileo Galilei was amongst the first observers of the early 17th century to provide an estimate of the Sun's rotational period by observing the sunspots being carried across the stellar disk by the star's rotation (Casas et al. 2006). When the stellar surface is not resolved, starspots still modulate the star's luminosity in a periodic way. Hence, the recording of the photometric light curve and the detection of a periodically modulated signal provide a direct estimate of the star's rotational period P_{rot}. This technique has the advantage over spectroscopy of yielding a measurement of the stellar rotation rate that is free of geometric effects and is straighforwardly converted to angular velocity, $\Omega = 2\pi/P_{rot}$. However, this is at the expense of requiring intense photometric monitoring over several rotational periods and applying dedicated signal processing techniques in order to recover the periodic component of the light curve that truly corresponds to the star's rotational period (e.g. Irwin et al. 2009).

This technique recently flourished with the Corot and Kepler satellites that acquired continuous stellar light curves of exquisite precision over timescales of months to years (e.g. Affer et al. 2012; McQuillan et al. 2013). The large number of rotational cycles recorded by these light curves allows not only the stellar rotational period to be derived with extreme accuracy but also to detect latitudinal differential rotation by traking spots located at different latitudes that have slightly different rotational periods (e.g. Mosser et al. 2009). The application of this technique is obviously most suited to magnetically active stars that exhibit starspots at their surface, i.e, usually solar-type and lower mass stars with a spectral type from late-F to M, extending even to brown dwarfs (e.g. Herbst et al. 2007).

2.4   Sismology

The oscillation spectrum of a star encodes its rotational properties from the surface down to the deep interior. To first order, the oscillation frequencies of radial order n, degree l, and azimuthal order m of a rotating star are related to the same frequencies in a non-rotating star by:

$$\nu_{n,l,m} = \nu_{n,l} - m\nu_s$$

where $m \in [-l, +l]$ and $\nu_s \simeq \nu_{rot} = \Omega/2\pi$ (Goupil et al. 2004). Stellar rotation lifts the m-degeneracy of the oscillation modes of a non-rotating star by producing a rotational splitting whose amplitude is directly proportional to angular velocity. In case of uniform rotation, the rotational splitting of the modes provides a direct measurement of surface angular velocity. For more complex rotational profiles, modeling the frequency splitting with rotating stellar models offers a way to estimate the internal rotation profile of the star. This technique was first applied to the Sun to recover the latitudinal and radial variations of the solar rotation rate through the convective envelope and down into the radiative core (e.g., Schou et al. 1998). More recently, a similar approach based on the analysis of the rotational splitting of mixed pressure and gravity modes allowed Deheuvels et al. (2012) to probe the internal rotation profile of a low-mass giant evolving off the main sequence, thus revealing a rapidly rotating inner core.

Additional information can be retrieved from the amplitude of the rotationally splitted modes. For instance, the ratio of the amplitudes of the $m = 0, \pm 1$ mode components depends on the inclination of the rotational axis on the line of sight (Gizon & Solanki 2003). A first application of this technique has recently allowed Chaplin et al. (2013) to demonstrate that the rotational axis of 2 transiting exoplanet hosts detected by Kepler is perpendicular to the orbital plane of the planets.

3   The rotational properties of solar-type and lower mass stars

We review in this section the rotational properties of stars with a mass less than $1.2M_\odot$, from early studies to the most recent determinations of rotational period distributions ranging from the early pre-main sequence (PMS) to the end of the main sequence (MS). The definition of physical quantities related to stellar rotation that we use in this Section are summarized in Table 1. Solar values are listed for reference.

3.1   Early studies and concepts

3.1.1   Rotation on the Main Sequence

Kraft (1970) provided one of the first reviews on the rotational properties of stars on the main sequence. The main characteristics of the rotation rate distribution was a sharp break in velocity at a spectral type around F4, i.e., around a mass

Table 1. Definitions of physical quantities related to stellar rotation.

Quantity	Symbol	Units	Solar value
Projected linear velocity	$v \sin i = V_{eq} \sin i$	km s^{-1}	$V_{eq,\odot} \simeq 1.9$ km s^{-1}
Rotational period	$P_{rot} = \frac{2\pi R_*}{V_{eq}}$	days	$P_{eq,\odot} \simeq 26$ d
Angular velocity	$\Omega_* = \frac{V_{eq}}{R_*} = \frac{2\pi}{P_{rot}}$	s^{-1}	$\Omega_\odot = 2.8 \ 10^{-6}$ s^{-1}
Critical velocity	$V_{crit} = \sqrt{\frac{2}{3}\frac{GM_*}{R_*}}$	km s^{-1}	$V_{crit,\odot} \simeq 360$ km s^{-1}
Latitudinal differential rotation	$\Omega(\theta) = \Omega_{eq} - \Delta\Omega \sin^2\theta$	s^{-1}	$\Delta\Omega_\odot = 4.8 \ 10^{-7}$ s^{-1}
Moment of inertia	$I = \frac{8\pi}{3}\int_0^{R_*} r^4\rho(r)dr$	g cm^2	$I_\odot = 6.4 \ 10^{53}$ g cm^2
Angular momentum	$J = \frac{8\pi}{3}\int_0^{R_*} r^4\rho(r)\omega(r)dr$	g cm^2 s^{-1}	$J_\odot^\dagger = 1.8 \ 10^{48}$ g cm^2 s^{-1}
Specific angular momentum	$j = (J/M)$	cm^2 s^{-1}	$j_\odot = 9 \ 10^{14}$ cm^2 s^{-1}
	N.B. If $\omega(r) = \Omega_*$, $J = I\Omega_* = k^2 M_* R_*^2 \Omega_*$, where kR_* is the stellar radius of gyration[‡]		$k^2_{conv,\odot} = 0.008$ $k^2_{rad,\odot} = 0.061$

[†] Pinto et al. (2011); [‡] cf. Ruciński (1988)

of ~ 1.2 M$_\odot$, with more massive stars having mean rotation rates of order of 100-200 kms^{-1}, while lower mass stars had much lower rotational velocities of order of a few kms^{-1}. The sharp decline of rotation rate for stars with deep convective envelopes had readily been interpreted by Schatzman (1962) as the result of angular momentum loss due to magnetized winds. In this framework, all stars were born with high rotation rates, and only magnetically active stars with surface convective envelopes would undergo strong braking as angular momentum is removed from their surface by magnetized stellar winds. In magnetically active stars, the ionised outflow remains coupled to the magnetic field out to a distance where the magnetic tension becomes unable to compensate for Coriolis force, i.e.:

$$r \simeq \frac{B^2}{16\pi\omega v\rho}$$

where B is the magnetic field intensity, ω the surface angular velocity, v the poloidal velocity of the wind flow, and ρ its density. The magnetic lever arm up to this radius yields angular momentum loss rates that are orders of magnitude larger than in the absence of magnetically-coupled winds. As shown by Weber & Davis (1967), the angular momentum loss rate can be expressed as:

$$\frac{dJ}{dt} = \frac{2}{3}\Omega\dot{M}r_A^2 = \frac{J}{\tau_W} \qquad (3.1)$$

where Ω is the stellar angular velocity, $\dot{M}$ the mass-loss rate, r_A the Alfvén radius, and τ_W the braking timescale. For the Sun, the Alfvén radius is about 30 times

larger than the solar radius, which translates into a braking timescale by the magnetized wind of order of 1 Gyr, i.e., short enough to account for the slow rotation of the Sun on the mid-main sequence.

A spectacular confirmation of this magnetic wind braking concept came with one of the first studies of rotational evolution among main sequence stars. Based on an earlier suggestion by Kraft (1967), Skumanich (1972) used published measurements of the mean rotation rate of solar-type stars in 2 young open clusters, the Pleiades and the Hyades, and comparing them to the Sun's rotation, derived his famous time-dependent velocity relationship $V_{eq} \propto t^{-1/2}$, for ages between 0.1 and 5 Gyr. This relationship is indeed what is asymptotically expected from the magnetic wind braking process, as shown by Durney & Latour (1978). Combining the following expression for mass-loss:

$$\dot{M} = -4\pi \rho_a u_a r_a^2 \qquad (3.2)$$

where ρ_a and u_a are the density and poloidal velocity of the outflow at the Alfvén radius r_a, with the definition of Alfvén velocity:

$$B_a^2 = 4\pi \rho_a u_a^2 \qquad (3.3)$$

where B_a is the stellar magnetic field at the Alfvén radius, and with the condition of magnetic flux conservation:

$$B_o r_o^2 = B_a r_a^2 \qquad (3.4)$$

and replacing the expressions above in Eq. 3.1, yields:

$$\frac{dJ}{dt} = \frac{2\Omega}{3u_a}(B_o r_o^2)^2 \qquad (3.5)$$

Further assuming that the poloidal velocity of the outflow at the Alfvén radius reaches the escape velocity $(u_a = v_{esc})$ and that the stellar magnetic field is powered by an internal dynamo process wich scales as $B_o \propto \Omega$, finally yields:

$$\frac{dJ}{dt} \propto \Omega^3 = I\frac{d\Omega}{dt} \qquad (3.6)$$

which asymptotically integrates to $\Omega \propto t^{-1/2}$, i.e., the Skumanich relationship. While extremely satisfying conceptually, this derivation makes a number of symplifying assumptions including spherically symmetric radial magnetic field and wind, thermally-driven outflows, and linear dynamo relationship, none of which strictly apply to active young stars (see Section 4).

As $v\sin i$ measurements accumulated in the mid-80's especially for stars located close to or on the zero-age main sequence (ZAMS) at an age of about 100 Myr, it became clear that, at these young ages, a large dispersion of rotation rates exists for solar-type and lower mass stars. Thus, Stauffer (1987) reported $v\sin i$ ranging from less than 10 kms^{-1} up to more than 150 kms^{-1} for G and K-type stars in the Alpha Persei (80 Myr) and Pleiades (120 Myr) young open clusters, at the start of

their main sequence evolution. Clearly, this unexpectedly large scatter of rotation rates at ZAMS pointed to a rotational evolution during the pre-main sequence that was far more complex than envisioned from the Skumanich relationship on the main sequence.

3.1.2 Rotation during the Pre-Main Sequence

Extrapolating the Skumanich relationship back in time to the pre-main sequence (PMS), at an age of $\sim$1 Myr, would predict rotational velocities of order of 200 kms^{-1}. Additionally, if protostellar collapse is dominated by gravity, one should expect protostars to rotate close to their break-up velocity. It therefore came as a surprise when the first measurements of rotational velocities for solar-mass PMS stars revealed that their rotation rate rarely exceeds 25 kms^{-1}, i.e., about a tenth of the break-up velocity (Vogel & Kuhi 1981; Bouvier et al. 1986; Hartmann et al. 1986). Even deeply embedded protostars appear to exhibit quite moderate rotation, with a mean value of about 40 kms^{-1} (Covey et al. 2005). Clearly, significant angular momentum loss must occur during protostellar collapse and/or during the embedded protostellar phase of evolution to account for such low rotation rates as the stars first appear in the HR diagram (see Hennebelle, this volume; Belloche, this volume). Like on the main sequence, higher mass PMS stars exhibit larger rotational velocities than their lower-mass counterparts (Dahm et al. 2012). Most of the so-called Herbig Ae-Be stars actually have similar velocities than their MS counterpart, which suggests they lose little angular momentum during the PMS, except for the precursors of the peculiar subgroup of magnetic A and B stars (cf. Alecian et al. 2013).

The low rotation rates of PMS low-mass stars is even more surprising when considering that they accrete high specific angular momentum material from their circumstellar disk for a few million years (Hernandez et al. 2007). As shown by Hartman & Stauffer (1989), a star accreting at a rate $\dot{M}$ from its disk will gain angular momentum at a rate:

$$\frac{dJ}{dt} = \dot{M} R_*^2 \Omega_{Kep} \tag{3.7}$$

where Ω_{Kep} is the Keplerian velocity of the disk material. It is then expected to spin up to an equatorial velocity of:

$$V_{eq} \simeq \frac{R_*^2 \int \dot{M} dt}{I} \cdot V_{br} \tag{3.8}$$

where $I \simeq 0.2 M_* R_*^2$ is the stellar moment of inertia and V_{br} the break-up velocity. Thus, for a mass accretion rate of a few 10^{-8} M$_\odot$yr^{-1} lasting for about 3 Myr, one expects the young star to rotate at more than half the break-up velocity. Clearly, since most low-mass PMS stars have much slower rotation rates, the accretion of high angular momentum material from the disk must be balanced by a process that efficiently removes angular momentum from the central star.

Based on a physical process thought to be at work in compact magnetized objects such as accreting neutron stars, Königl (1991) was first to suggest that the magnetic interaction between the inner disk and a young magnetized star might provide a way to remove part of the angular momentum gained from accretion. Shortly after, evidence for a correlation between rotation rate and accretion was reported (Bouvier et al. 1993; Edwards et al. 1993), with accreting young stars rotating on average more *slowly* than non-accreting ones, thus providing a strong support to Königl's suggestion. Yet, more than 20 years later, the controversy is still very much alive as to whether the magnetic star-disk interaction is efficient enough to counteract the accretion-driven angular momentum gain in young stars (see Ferreira, this volume). Also, even though a number of recent studies appear to confirm the early evidence for a rotation-accretion connection in young stars (e.g. Rebull et al. 2006; Cieza & Baliber 2007; Cauley et al. 2012; Dahm et al. 2012; Affer et al. 2013), some discrepant results have also been reported (e.g. Le Blanc et al. 2011). Thus, while there is a general consensus for young accreting stars being somehow prevented from spinning up as they evolve towards the main sequence (e.g., Rebull et al. 2004), the underlying physical mechanism responsible for this behaviour is not totally elucidated yet.

3.2 Recent developments

While the early studies from the 60's to the 80's mostly focused on the determination of projected rotational velocities, $v \sin i$, large-scale photometric monitoring campaigns started in the 90's that provided complete rotational period distributions for thousands of low-mass stars in the PMS and MS stages. Figure 2 (from Irwin & Bouvier 2009, see references therein) illustrates a compilation of some of these results. It shows how the distribution of rotational periods evolves from the start of the PMS at about 1 Myr to the mid-MS at 0.6 Gyr. A number of clear evolutionary trends emerge, which have been confirmed by more recent studies. The initial distribution in the Orion Nebulae Cluster at $\simeq 1$ Myr is quite broad. It was found to be bimodal for stars more massive than 0.3 $M_{\odot}$ with a slow rotator peak with periods around 8 days and a fast rotator group with periods around 2 days (Herbst et al. 2001). The peak of slow rotators is usually attributed to PMS stars still interacting with their disk, hence being prevented from spinning up, while the fast rotators are thought to mainly consist of stars that have already dissipated their circumstellar disks and therefore have started to spin up as they evolve towards the ZAMS. In constrast, the rotational period distribution of very low-mass stars appears unimodal and skewed towards faster rotators. As time progresses towards the ZAMS, which is reached in about 40 Myr for a solar-mass star and 150 Myr for a 0.5 $M_{\odot}$ star, the period distributions evolve towards faster rotation, especially in the low mass domain where rotational periods at ZAMS converge to values less than 1 day. However, for stars more massive than about 0.4 $M_{\odot}$, a large dispersion of rotation rates remains up to the ZAMS. It is only later on the MS, by an age of about 0.5 Gyr, that all but the lowest mass stars are significantly braked, to reach periods larger than about 10 days (Delorme et
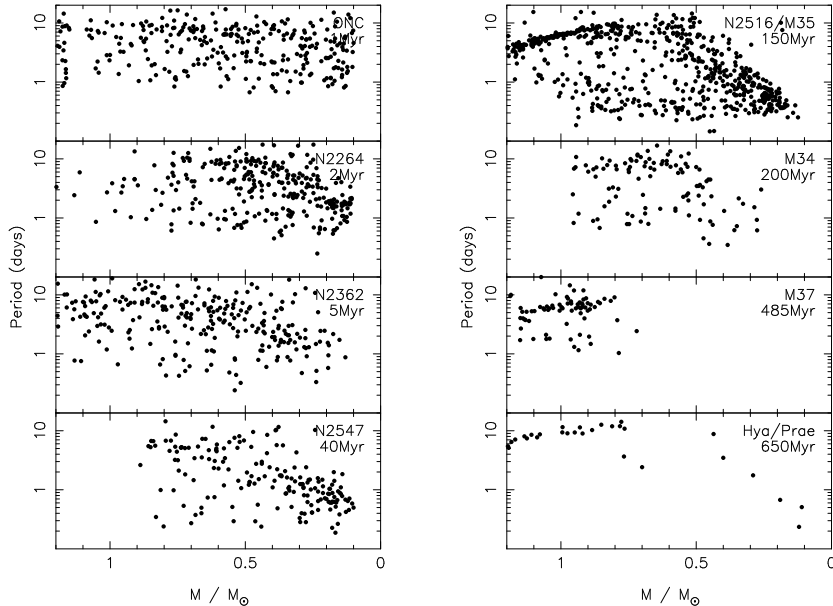
Fig. 2. Compilation of several thousands rotation periods for stars with masses M≤1.2 M⊙ in young clusters in the age range from 1 Myr to 0.6 Gyr. Plotted in each panel is rotation period as a function of stellar mass for a single cluster or from combined clusters when they have similar ages (e.g. NGC 2516/M35, Hyades/Praesepe). From Irwin & Bouvier (2009).

al. 2011; Meibom et al. 2011), and exhibit a tight rotation-mass relationship. At the low mass end, below 0.6 M⊙, a significant dispersion still subsists at that age (Scholz et al. 2011; Agüeros et al. 2011) and even beyond for most late-type field dwarfs (McQuillan et al. 2013), lasting for perhaps as long as 10 Gyr for the lowest mass stars (M≤0.3 M⊙; Irwin et al. 2011). Hence, the spin down timescale on the main sequence significantly increases towards lower mass objects, from a few 0.1 Gyr for solar-type and low-mass stars up to a few Gyr for very low-mass stars (Delfosse et al 1998).

These recent studies have highlighted that the angular momentum (AM) evolution of cool stars is strongly mass dependent, both during the PMS and on the MS, as can be clearly seen from Fig. 2. Schematically, solar-type and low-mass stars (0.5-1.1 M⊙) have a large initial dispersion of rotational periods that subsists and even widens to the ZAMS, and is eventually erased on the MS as all stars in this mass range are efficiently braked on a timescale of a few 0.1 Gyr, thus yielding a well-defined rotation-mass sequence with little scatter. The rotational

convergence of solar-type stars on the early MS has led to the developement of gyrochronology, i.e., the measurement of stellar age from rotation rate (e.g., Barnes 2003; Delorme et al. 2011; Epstein & Pinsonneault 2012). In contrast, very low-mass stars (M$\leq$0.3 M$_\odot$), while also exhibiting some dispersion of rotation rates at the start of the PMS evolution, seems to all converge towards fast rotation at ZAMS, and resume building up a large rotational scatter on a timescale of a few Gyr on the MS. This different behaviour is well illustrated by the changing shape of the period-mass diagrams shown in Fig 2 as time goes by.

Going deeper into the mass spectrum, brown dwarfs' (BD's, M$\leq$0.08 M$_\odot$) rotational properties seem to mimic and extend those of very low-mass stars (Herbst et al. 2007; Rodríguez-Ledesma et al. 2009), with no apparent rotational discontinuity at the stellar/substellar boundary. As a group, they tend to rotate faster than stars at all ages (Mohanty & Basri 2003), with a median period of order of 15 hours at young ages, and some indeed with rotational periods as short as a few hours, i.e., reaching close to the rotational break-up (Scholz & Eislöffel 2004, 2005). Rapid rotation is still measured for evolved BD's at an age of a few Gyr, which suggests that they suffer much weaker angular momentum losses than stars (Reiners & Basri 2008).

4 Modeling the angular momentum evolution of cool stars

The wealth of new data acquired since the mid-90's, now encompassing several thousands of rotational periods measured for cool stars over an age range covering from the start of the PMS to the late-MS prompted renewed interest in the development of angular momentum evolution models. While a review of all existing models and their origin is far beyond the scope of this introductory course, we outline in this section the main physical processes that are thought to drive the rotational evolution of low-mass stars and how they are currently implemented in parametrized models of angular momentum evolution.

4.1 The physical processes behind rotational evolution

The rotational evolution of low-mass stars is believed to be dictated by 3 main physical processes: star-disk interaction in the early PMS, magnetized wind braking, and AM transport in the stellar interior. We only briefly summarize these processes below, as they are reviewed in much more detailed in other contributions to this volume.

4.1.1 Star-disk interaction during the early PMS

Camenzind (1990) and Königl (1991) were first to suggest that the low rotation rates of PMS stars may result from the magnetic star-disk interaction. The picture envisioned at that time was inspired by the Ghosh et al.'s (1977) model developed for accreting neutron stars (e.g. Collier Cameron et al. 1995). While this model now does not seem to be efficient enough to apply to young stars, a number of

alternatives have been proposed still relying on the inner disk interacting with a strong stellar magnetosphere. Indeed, young stars are known to host strong magnetic fields (cf. Donati, this volume) that are able to disrupt the inner disk regions and channel the accretion flow onto the star through magnetic funnels (cf. Bouvier et al. 2007 for a review). Bessolaz et al. (2008) derived the following expression for the magnetospheric truncation radius:

$$\frac{r_{tr}}{R_*} \simeq 2m_s^{2/7} \left(\frac{B_*}{140G}\right)^{4/7} \left(\frac{\dot{M}_a}{10^{-8}M_\odot yr^{-1}}\right)^{-2/7} \left(\frac{M_*}{0.8M_\odot}\right)^{-1/7} \left(\frac{R_*}{2R_\odot}\right)^{5/7} \quad (4.1)$$

where m_s is the sonic Mach number at the disc midplane, B_* the stellar magnetic field, and $\dot{M}_a$ the mass accretion rate. For values of the parameters relevant to a young accreting solar-mass system, the magnetospheric truncation radius is located a few stellar radii above the stellar surface, a prediction borne out by observations (e.g. Najita et al. 2007). This distance is of the same order as the disk corotation radius, i.e., the radius at which the keplerian angular velocity in the disk equals the star's angular velocity:

$$r_{co} = \left(\frac{GM_*}{\Omega_*^2}\right)^{1/3} \quad (4.2)$$

The net flux of angular momentum exchanged between the star and the disk strongly depends upon whether the magnetospheric truncation radius is located within or beyond the disk corotation radius. Therefore, the changing magnetic topology of solar-type stars evolving on their convective and radiative PMS tracks will most likely impact their early rotational evolution (e.g. Gregory et al. 2012).

Within this general framework, various scenarios have been developed to attempt to produce a negative net angular momentum torque onto the star, so as to explain why young stars are slow rotators in spite of both accretion and contraction. These include accretion-driven winds (Matt & Pudritz 2008), X-winds and their variants (Mohanty and Shu 2008; Ferreira et al. 2000) , and magnetospheric ejections (Zanni & Ferreira 2013). These models are discussed at length in J. Ferreira's contribution to this volume. Whether any of these processes is actually able to counteract the spin up due to accretion and contraction during the early PMS is, however, unsettled. Pending a satisfactory model for PMS spin down, most current angular momentum evolution models assume that accreting PMS stars evolve at constant angular velocity (cf. Sect. 4.2).

4.1.2 Rotational braking by magnetized winds

Starting from the general expression of angular momentum loss due to magnetized stellar winds (Eq. 3.1 above), Kawaler (1988) worked out a parametrized formulation that can be straightforwardly implemented in evolutionary models. Following Mestel (1984), the AM loss rate is given by:

$$\dot{J}_{\rm W} = \frac{2}{3}\dot{M}\Omega_* R_*^2 \left[\left(\frac{r_A}{R_*}\right)_{radial}\right]^n \quad (4.3)$$

where $\dot{M}$ is the mass loss rate, Ω_* the stellar angular velocity, R_* the stellar radius, r_A the Alfvén radius, and the exponent n reflects the magnetic field geometry with $n = 2$ for a radial field and $n = 3/7$ for a dipolar field. From Eq. 3.2, 3.3, and 3.4 above, the expression of the Alfvén radius is given by:

$$\left(\frac{r_A}{R_*}\right)^2_{radial} = \frac{B_*^2 R_*^2}{\dot{M} u_a} \tag{4.4}$$

where B_* is the stellar magnetic field intensity, and u_a the flow velocity at the Alfvén radius. Further assuming that the flow velocity at the Alfvén radius is of order of the escape velocity, and adding a dynamo relationship for the generation of the stellar magnetic field of the form:

$$B_* R_*^2 \propto \Omega_*^a \tag{4.5}$$

where a is the dynamo exponent, finally leads to:

$$\dot{J}_{\mathrm{W}} = -K_{\mathrm{W}} \dot{M}^{1-(2n/3)} \Omega_*^{1+(4an/3)} R_*^{2-n} M_*^{-n/3} \tag{4.6}$$

For an asumed linear dynamo relationship ($a=1$), and a magnetic topology intermediate (in some sense) between a radial and a dipolar field with $n=1.5$, Eq.4.6 simplifies to:

$$\dot{J}_{\mathrm{W}} = -K_{\mathrm{W}} \Omega_*^3 R_*^{1/2} M_*^{-1/2} \tag{4.7}$$

which is easily implement in an evolutionary model. Direct application of this prescription, however, proved to produce too strong braking for fast rotators compared to observations (Stauffer & Hartmann 1987). Most models have therefore adopted a variant of Kawaler's prescription, first proposed by Chaboyer et al. (1995), that assumes that the dynamo saturates ($a = 0$) above some angular velocity ω_{sat}, i.e.:

$$\dot{J}_{\mathrm{W}} = \begin{cases} -K_{\mathrm{W}} \Omega_*^3 R_*^{1/2} M_*^{-1/2} & \Omega \leq \omega_{sat} \\ -K_{\mathrm{W}} \Omega_* \omega_{sat}^2 R_*^{1/2} M_*^{-1/2} & \Omega_* > \omega_{sat} \end{cases} \tag{4.8}$$

The shallower slope of the rotation-dependent angular momentum loss at high rotation, i.e., $\dot{J}_{\mathrm{W}} \propto \Omega$ instead of $\dot{J}_{\mathrm{W}} \propto \Omega^3$, provides a better agreement with the observation of very fast rotators at the ZAMS. Magnetic field measurements suggest that dynamo saturation occurs at a fixed Rossby number $R_0 \simeq 0.1$ in cool stars (Reiners et al. 2009; Wright et al. 2011), with $R_0 = 2\pi(\omega \tau_c)^{-1}$ where τ_c is the turnover convective time. As τ_c lengthens towards lower mass stars, w_{sat} is expected to decrease with mass, i.e., lower mass stars suffer less angular momentum loss than solar-type ones. This Rossby scaling thus naturally accounts for the longer spin down timescale of lower mass stars on the main sequence (Krishnamurthi et al. 1997; Bouvier et al. 1997). However, Sills et al. (2000) showed that very low-mass stars ($M \leq 0.4$ $M_\odot$) experience much less spin down than the extrapolation of the Rossby scaling to very low masses would predict. Recently, Reiners & Mohanty (2012) proposed a modification to Kawaler's prescription, based on a more physically-funded dynamo relationship, that appears to alleviate this issue.

Recent MHD numerical simulations of stellar winds have considerably improved our understanding of wind-driven angular momentum loss (e.g. Aarnio et al. 2012; Vidotto et al. 2009, 2011). Based on 2D numerical simulations of MHD winds originating from stars with a dipolar magnetic field, Matt et al. (2012) derived the following expression for the Alfvén radius:

$$\frac{r_A}{R_*} = K_1 \left[\frac{\Upsilon}{(K_2^2 + 0.5f^2)^{1/2}} \right]^m \qquad (4.9)$$

where f is the ratio of the stellar rotation rate to the break-up velocity and

$$\Upsilon = \frac{B_*^2 R_*^2}{\dot{M}_{\mathrm{W}} v_{esc}} \qquad (4.10)$$

where B_* is the magnetic field strength at the stellar equator, $\dot{M}_{\mathrm{W}}$ the wind mass loss rate, and v_{esc} the escape velocity. The value of the constants appearing in Eq. 4.9 are derived from numerical simulations that explore the parameter space, yielding $K_1 = 1.3$, $K_2 = 0.0506$ and $m = 0.2177$. Provided the stellar magnetic field can be tied to the angular velocity through a dynamo prescription, and the wind mass loss rate can be computed as a function of stellar rotation and other fundamental stellar parameters (e.g. Cranmer & Saar 2011), the expression given by Eq. 4.9 for the Alfvén radius can be implemented in Eq. 3.1 to compute the amount of wind-driven angular momentum losses during stellar evolution. Models using this new prescription for AM losses are illustrated below (cf. Sect. 4.2).

4.1.3   Angular momentum transport in stellar interiors

As angular momentum is carried away by stellar winds at the stellar surface, several mechanisms may operate to redistribute angular momentum in the stellar interior. These range from various classes of hydrodynamical instabilites (e.g. Lagarde et al. 2012, see also the contributions of Palacios and Rieutord in this volume), magnetic fields (e.g. Eggenberger et al. 2005), and gravity waves (Talon & Charbonnel 2008; Charbonnel et al. 2013; see also Mathis, this volume). The recent report of rapidly rotating cores in red giants from asterosismology (e.g. Mosser et al. 2012) and the discrepancy between the measured angular velocity gradient and model expectations indicate that angular momentum transport mechanisms in stellar interiors are still not totally elucidated (e.g. Eggenberger et al. 2012).

Lacking a detailed physical modeling of the processes involved, MacGregor & Brenner (1991) introduced a parametrized prescription for angular momentum transport between the radiative core and the convective envelope. Each region is considered as rotating uniformly but not necessarily at the same rate, as the convective envelope is slowed down. They assumed that AM transport processes would act to erase angular velocity gradients at the boundary between the radiative core and the convective envelope (the tachocline, cf. Spiegel & Zahn 1992), on a timescale τ_{ce}, the so-called core-envelope coupling timescale. To reach a state of uniform rotation on a timescale τ_{ce} throughout the star, a quantity ΔJ of angular

momentum has to be exchanged between the radiative core and the convective envelope, with:

$$\Delta J = \frac{I_{conv}J_{core} - I_{core}J_{conv}}{I_{core} + I_{conv}} \tag{4.11}$$

where I_{conv}, I_{core} and J_{conv}, J_{core} are the moment of inertia and the angular momentum content of the convective envelope and the radiative core, respectively. Then, the angular momentum evolution of the radiative core and the convective envelope can be written as:

$$\frac{dJ_{core}}{dt} = -\frac{\Delta J}{\tau_{ce}} \tag{4.12}$$

and

$$\frac{dJ_{conv}}{dt} = \frac{\Delta J}{\tau_{ce}} - \frac{J_{conv}}{\tau_J} \tag{4.13}$$

where τ_J is the wind braking timescale[1]. This prescription has been used in two-zone angular momentum evolution models (e.g. Allain 1998) that provide some insight into the value of τ_{ce} and its dependence upon rotation rate and stellar parameters. A short coupling timescale corresponds to an efficient AM redistribution and leads to solid-body rotation, while a long τ_{ce} allows for strong angular velocity gradients to develop at the tachocline as the star evolves. Thus, this parametrization offers some empirical guidance to identify the actual underlying physical mechanisms at work for angular momentum transport in stellar interiors based on the timescales involved.

4.2 Parametrized models of angular momentum evolution

Angular momentum evolution models have been developed in an attempt to reproduce the run of surface rotation as a function of time, as derived from observations for solar-type stars, low-mass and very low-mass stars. In this section, we illustrate a class of semi-empirical models that use parametrized prescriptions to implement the physical processes described in the previous section.
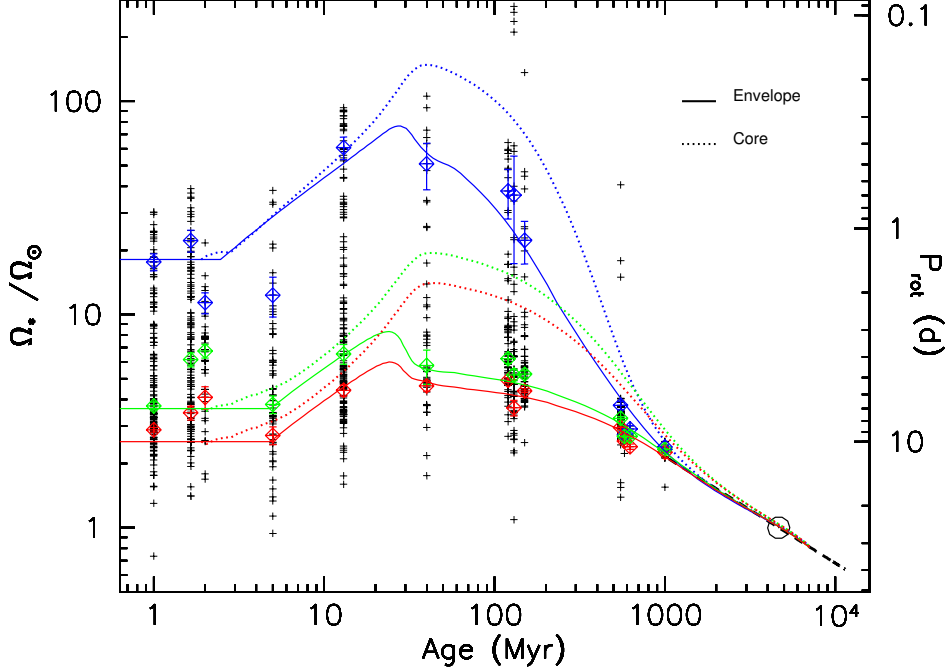
4.2.1 Solar-type stars

Figure 3 (from Gallet & Bouvier 2013) illustrates the observed and modeled angular momentum evolution of solar-type stars, in the mass range 0.9-1.1 M$_\odot$, from the start of the PMS at 1 Myr to the age of the Sun. The rotational distributions of solar-type stars are shown at various time steps corresponding to the age of the star forming regions and young open clusters to which they belong (see Fig.2). Three models are shown, which start with initial periods of 10, 7, and 1.4 days, corresponding to slow, median, and fast rotators. The models assume constant angular velocity during the star-disk interaction phase in the early PMS

---

[1]Note that during the pre-main sequence, additional terms enter the above equations governing the evolution of the core and envelope angular momenta as the radiative core develops in the initially fully convective star (cf. Allain 1998).

Fig. 3. The rotational angular velocity of solar-type stars is plotted as a function of age. The left y-axis is labelled with angular velocity scaled to the angular velocity of the present Sun while the right y-axis is labelled with rotational period in days. On the x-axis the age is given in Myr. *Observations:* The black crosses shown at various age steps are the rotational periods measured for solar-type stars in star forming regions and young open clusters over the age range 1 Myr-1 Gyr. The associated red, green, and blue diamonds represent the 25, 50, and 90th percentiles of the observed rotational distributions. The open circle at 4.56 Gyr is the angular velocity of the present Sun. *Models:* The angular velocity of the convective envelope (solid line) and of the radiative core (dashed lines) is shown as a function of time for slow (red), median (green), and fast (blue) rotator models, with initial periods of 10.0, 7.0, and 1.4 days, respectively. The dashed black line at the age of the Sun illustrates the asymptotic Skumanich's relationship, $\Omega \propto t^{-1/2}$. From Gallet & Bouvier (2013).

(cf. 4.1.1), implement the Matt et al. (2012) wind braking prescription (cf. 4.1.2), as well as core-envelope decoupling (cf. 4.1.3). The free parameters of the models are the initial periods, scaled to fit the rotational distributions of the earliest clusters, the star-disk interaction timescale τ_d during which the angular velocity is held constant at its initial value, the core-envelope coupling timescale τ_{ce}, and the calibration constant K_1 for wind-driven AM losses. The latter is fixed by the requirement to fit the Sun's angular velocity at the Sun's age. These parameters

are varied until a reasonable agreement with observations is obtained. In this case, the slow, median, and fast rotator models aim at reproducing the 25, 50, and 90th percentiles of the observed rotational distributions and their evolution from the early PMS to the age of the Sun.

The models provide a number of insights into the physical processes at work. The star-disk interaction lasts for a few Myr in the early PMS, and possibly longer for slow rotators ($\tau_d \simeq 5$ Myr) than for fast ones ($\tau_d \simeq 2.5$ Myr). As the disk dissipates, the star begins to spin up as it contracts towards the ZAMS. The models then suggest much longer core-envelope coupling timescales for slow rotators ($\tau_{ce} \simeq 30$ Myr) than for fast ones ($\tau_{ce} \simeq 12$ Myr). Hence, once they have reached the ZAMS, slow rotators exhibit much lower surface velocities than fast rotators but significantly larger angular velocity gradients at the tachocline. Indeed, most of the initial angular momentum is hidden in the core of the slow rotators at ZAMS. As they evolve on the early MS, wind braking eventually leads to the convergence of rotation rates for all models by an age of $\simeq 1$ Gyr, to asymptotically reach the Skumanich's relationship. These models thus clearly illustrate the different rotational histories solar-type stars may experience, depending mostly on their initial period and disk lifetime. In turn, the specific rotational history a star undergoes may strongly impact on its properties, such as lithium content, even long after rotational convergence has taken place (cf. Bouvier 2008; Randich 2010).

The models discussed above describe the rotational evolution of single stars while many cool stars belong to multiple stellar systems. In short period binaries ($P_{orb} \leq 12$ days), tidal interaction will enforce synchronization betweeen the orbital and rotational period (Zahn 1977). Clearly, the rotational evolution of the components of such systems is totally different from that of single stars, and rapid rotation is usually maintained over the whole main sequence (Zahn & Bouchet 1989) and even beyond, like in, e.g., the magnetically-active rapidly-rotating RS CVn systems. However, the fraction of such tight, synchronized systems among solar-type stars is low, of order of 3% (Raghavan et al. 2010), so that tidal effects are unlikely to play a major role in the angular momentum evolution of most cool stars.

Presumably much more frequent is the occurrence of planetary systems around solar-type and low-mass stars (e.g. Mayor et al. 2011; Bonfils et al. 2013). The frequency of hot Jupiters, i.e., massive planets close enough to their host star to have a significant tidal influence[2] (cf. Dobbs-Dixon et al. 2004), is a mere 1% around FGK stars (e.g. Wright et al. 2012). However, there is mounting evidence that the planetary formation process is quite dynamic, with gravitational interactions taking place between forming and/or migrating planets (Albrecht et al. 2012). This may lead to planet scattering and even planet engulfment by the host star. The impact of such catastrophic events onto the angular momentum evolution of planet-bearing stars has been investigated by Bolmont et al. (2012) who showed it could be quite significant both during the PMS and on the main

---

[2]The magnetospheric interaction between the star and a hot Jupiter may also impact the stellar spin rate (cf. e.g. Lanza 2010; Cohen et al. 2010)
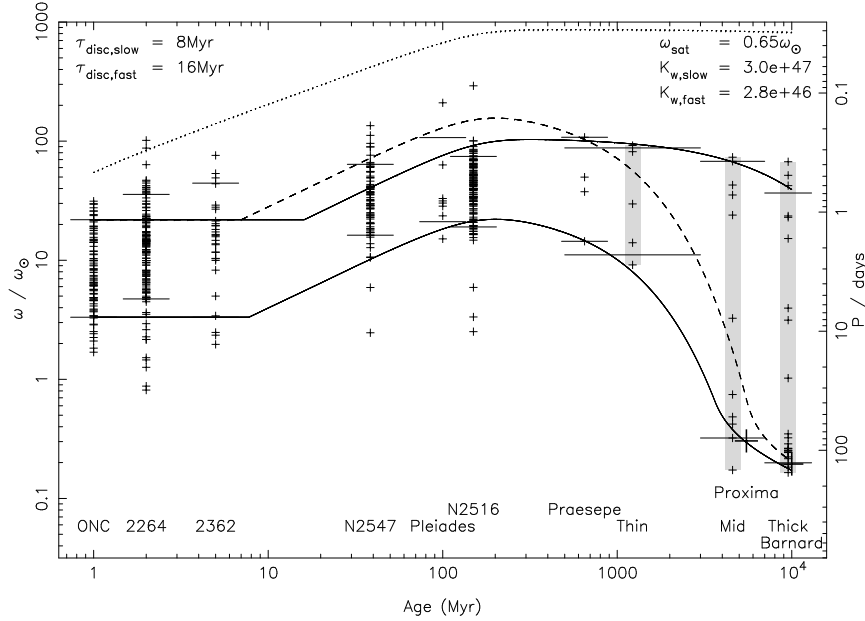
Fig. 4. The rotational angular velocity of very low-mass stars (0.1-0.35 M$_\odot$) is plotted as a function of age. The left y-axis is labelled with angular velocity scaled to the angular velocity of the present Sun while the right y-axis is labelled with rotational period in days. On the x-axis the age is given in Myr. *Observations:* The black crosses shown at various age steps are the rotational periods measured for very low-mass stars in star forming regions, young open clusters, and in the field over the age range 1 Myr-10 Gyr. Short horizontal lines show the 10th and 90th percentiles of the angular velocity distributions at a given age, used to characterize the slow and fast rotators, respectively. *Models:* The solid curves show rotational evolution models for 0.25 M$_\odot$ stars, fit to the percentiles, with the upper curve for the rapid rotators (with parameters $\tau_{d,fast}$ and K$_{W,fast}$) and the lower curve for the slow rotators (with parameters $\tau_{d,slow}$ and K$_{W,slow}$). Note the factor of 10 difference between K$_{W,fast}$ and K$_{W,slow}$. The dashed curve shows the result for the rapid rotators if the wind parameter K$_{W,fast}$ is assumed to be the same as for the slow rotators rather than allowing it to vary. The dotted curve shows the break-up limit. From Irwin et al. (2011).

sequence.

4.2.2   Very low-mass stars

Models similar to those described above for solar-type stars have been shown to apply to lower mass stars, at least down to the fully convective boundary ($\simeq$0.3 M$_\odot$), with the core-envelope coupling timescale apparently lengthening as the convective envelope thickens (e.g., Irwin et al. 2008). In the fully convective regime, i.e., below 0.3 M$_\odot$, models ought to be simpler as the core-envelope decoupling assumption becomes irrelevant and uniform rotation is usually assumed instead throughout the star. Yet, the rotational evolution of very low-mass stars actually appears more complex than that of their more massive counterparts and still challenges current models. Rotational period measurements for field M-dwarfs show a bimodal distribution with a peak of fast rotators in the period range 0.2-10 days, and a peak of slow rotators with rotational periods ranging from 30 days to at least 150 days (Irwin et al. 2011). Most of the slow rotators appear to be thick disk members, i.e., they are on average older than the fast ones that are kinematically associated to the thin disk. The apparent bimodality coud thus simply result from a longer spin down timescale of order of a few Gyr, as advocated by Reiners & Mohanty (2012).

However, as shown in Figure 4 (from Irwin et al. 2011), this bimodality may not be easily explained for field stars at an age of several Gyr. It is seen that the large dispersion of rotation rates observed at late ages for very low-mass stars requires drastically different model assumptions. Specifically, for a given model mass (0.25 M$_\odot$ in Fig. 4), the calibration of the wind-driven angular momentum loss rate has to differ by one order of magnitude between slow and fast rotators (Irwin et al. 2011). Why does a fraction of very low-mass stars remain fast rotators over nearly 10 Gyr while another fraction is slowed down on a timescale of only a few Gyr is currently unclear. A promising direction to better understand the rotational evolution of very low mass stars is the recently reported evidence for a bimodality in their magnetic properties. Based on spectropolarimetric measurements of the magnetic topology of late M dwarfs (Morin et al. 2010), Gastine et al. (2013) have suggested that a bistable dynamo operates in fully convective stars, which results in two contrasting magnetic topologies: either strong axisymmetric dipolar fields or weak multipolar fields. Whether the different magnetic topologies encountered among M dwarfs is at the origin of their rotational dispersion at late ages remains to be assessed.

5   The rotational properties of massive and intermediate-mass stars

As outlined in Sect. 3.1, stars more massive than 1.2 M$_\odot$ have significantly larger rotation rates than solar-type and low-mass stars. In comparison to low-mass stars, more massive stars have higher initial angular momenta, shorter contraction timescales to the ZAMS and shorter evolution timescales on the MS, they lack deep convective envelopes and strong magnetic fields (except for peculiar sub-classes, such as Ap-Bp stars), and drive dense radiative winds. For all these reasons, their rotational evolution is expected to be quite different from that of their low-mass

counterparts. We briefly review in the next sections the rotational properties of massive and intermediate-mass stars.

5.1 Massive stars (4-15 M$_\odot$)

Braganca et al. (2012) have recently summarized the rotational distributions of 350 nearby O9-B6 stars in the Galactic disk from $v \sin i$ measurements. After correcting for projection effect (i.e., $< V_{eq} > = \frac{4}{\pi} < V \sin i >$, cf. Gaigé 1993), they find that the mean equatorial velocity is of order of 125 kms^{-1} and relatively uniform over the whole mass range they probe. A similar study was performed by Huang & Gies (2006) for 496 O9-B9 stars belonging to 19 young open clusters yielding an average equatorial velocity of 190 kms^{-1}, i.e., significantly higher than the mean rotation rate of massive field stars. Specifically, the difference in mean velocity between cluster and field stars at high masses stems from the much smaller fraction of slow rotators observed in clusters, while the two populations have similar $v \sin i$ distributions above $\simeq$100 kms^{-1}. Even though cluster members are on average younger than field dwarfs, Meynet & Maeder (2000) rotating evolutionary models predict only modest spin down for massive stars on the main sequence, with a braking rate of order of 15-20% for 9-12 M$_\odot$ stars. Indeed, the comparison of massive field dwarfs and cluster members over the same age range (12-15 Myr) still result in differing average velocities, thus suggestive of an intrinsic rather than an evolutionary effect (Strom et al. 2005). Wolff et al. (2007) further confirmed that massive stars formed in high-density regions, e.g. rich clusters, lack the numerous slow rotators seen for stars of similar masses in low-density regions and the field. These authors suggested that the density-dependent rotational distribution observed for massive stars may reflect a combination of initial conditions, e.g., higher turbulence in massive proto-clusters yielding larger initial angular momenta, and environmental conditions, where the stronger ambient UV flux from O-type stars in rich clusters may shorten the disk lifetimes, thus minimizing the braking efficiency of the star-disk interaction during the early angular momentum evolution of massive stars. Yet, it is unclear whether the disk locking scenario discussed above for low-mass pre-main sequence stars does apply to more massive stars (cf. Rosen et al. 2012). Nevertheless, regardless of the actual physical processes at work, the observed relationship between the shape of the rotational distributions of massive stars and the specific properties of their birthplace seems to indicate that initial conditions have a long-lasting impact on their rotational properties.

5.2 Intermediate-mass stars (1.3-4 M$_\odot$)

As mentionned in previous sections (see 3.1.2), intermediate-mass PMS stars, the so-called Herbig Ae-Be stars, have on average much higher rotational velocities than their lower mass T Tauri counterparts at an age of a few Myr. Wolff et al. (2004) investigated the rotational evolution of intermediate-mass PMS stars (1.3-2 M$_\odot$) as they evolve from convective to radiative tracks towards the ZAMS.

Comparing the measured velocities on convective tracks to those of stars landing on the ZAMS over the same mass range, they concluded that angular momentum is conserved in spherical shells within the star, i.e., that the PMS spin up is directly proportional to the contraction of the stellar radius. The lack of angular momentum redistribution in the predominantly radiative interiors of intermediate-mass PMS stars would then imply that they develop a large degree of radial differential rotation from the center to the surface as they approach the ZAMS.

Further insight into the rotational properties and evolution of intermediate-mass stars is provided by the large-scale study of Zorec & Royer (2012) who reported $v \sin i$ measurements for 2,014 B6- to F2-type stars. By tracing the evolution of rotation as a function of age, they confirm that intermediate-mass stars seem to evolve on the main sequence as differential rotators. Striking differences between the rotational distribution of 1.6-2.4 $M_\odot$ stars and that of 2.4-3.8 $M_\odot$ stars, the former being unimodal while the latter is bimodal, remain to be understood. Similarly, the complex rotational behaviour of stars over this mass range as they evolve onto the MS, with an apparent spin up during the first half of the MS evolution followed by a significant spin down during the second half, represents a real challenge for angular momentum evolution models.

A specific sub-group of intermediate-mas stars, the magnetic Ap-Bp stars host surface magnetic fields of a few kG to a few 10 kG. This sub-group represents about 5-10% of the population and is known to exhibit systematic lower velocities that their non-magnetic counteparts (Abt & Morrell 1995). Alecian et al. (2012) showed that their precursors, i.e., the magnetic Herbig Ae-Be stars, already are slower rotators that non-magnetic intermediate-mass PMS stars, indicating that magnetic braking is already efficient during the PMS for this particuliar subgroup. As the spin down continues on the MS, Ap stars can reach very slow rotation indeed, with the longest rotational period ever reported amounting to 77±10 years (Leroy et al. 1994).

6 Conclusion

The last decade has seen tremendous progress in the characterization of the rotational properties of stars at various stages of evolution and over the whole mass range from brown dwarfs to the most massive objects. These new observational results bring formidable constraints to the development of angular momentum evolution models. While the dominant processes thought to dictate the rotational evolution of stars are probably identified, much remains to be done to understand their detailed physics and their respective roles. The confrontation between models and observations, though much improved in recent years, still indicate a number of shortcomings related to transport processes in radiative interiors, the physics of stellar winds, and the interaction between the star and its environment. Major advances are expected to arise from multi-dimensional numerical simulations of stellar interiors and stellar atmospheres, which will hopefully provide new clues to the elusive physical processes that govern the rotational evolution of stars from their birth to the last stages of their evolution.

References

Aarnio, A. N., Matt, S. P., & Stassun, K. G. 2012, ApJ, 760, 9

Abney, W. D. W. 1877, MNRAS, 37, 278

Abt, H. A., & Morrell, N. I. 1995, ApJS, 99, 135

Affer, L., Micela, G., Favata, F., & Flaccomio, E. 2012, MNRAS, 424, 11

Affer, L., Micela, G., Favata, F., Flaccomio, E., & Bouvier, J. 2013, MNRAS, 430, 1433

Agüeros, M. A., Covey, K. R., Lemonias, J. J., et al. 2011, ApJ, 740, 110

Albrecht, S., Winn, J. N., Johnson, J. A., et al. 2012, ApJ, 757, 18

Alecian, E., Wade, G. A., Catala, C., et al. 2013, MNRAS, 429, 1027

Allain, S. 1998, A&A, 333, 629

Baranne, A., Mayor, M., & Poncet, J. L. 1979, Vistas in Astronomy, 23, 279

Barnes, J. R., Collier Cameron, A., Donati, J.-F., et al. 2005, MNRAS, 357, L1

Barnes, S. A. 2003, ApJ, 586, 464

Benz, W., & Mayor, M. 1981, A&A, 93, 235

Benz, W., & Mayor, M. 1984, A&A, 138, 183

Bessolaz, N., Zanni, C., Ferreira, J., Keppens, R., & Bouvier, J. 2008, A&A, 478, 155

Bolmont, E., Raymond, S. N., Leconte, J., & Matt, S. P. 2012, A&A, 544, A124

Bonfils, X., Delfosse, X., Udry, S., et al. 2013, A&A, 549, A109

Bouvier, J. 2008, A&A, 489, L53

Bouvier, J., Forestini, M., & Allain, S. 1997, A&A, 326, 1023

Bouvier, J., Bertout, C., Benz, W., & Mayor, M. 1986, A&A, 165, 110

Bouvier, J., Alencar, S. H. P., Harries, T. J., Johns-Krull, C. M., & Romanova, M. M. 2007, Protostars and Planets V, 479

Bouvier, J., Cabrit, S., Fernandez, M., Martin, E. L., & Matthews, J. M. 1993, A&A, 272, 176

Bragança, G. A., Daflon, S., Cunha, K., et al. 2012, AJ, 144, 130

Camenzind, M. 1990, Reviews in Modern Astronomy, 3, 234

Carroll, J. A. 1933, MNRAS, 93, 478

Casas, R., Vaquero, J. M., & Vazquez, M. 2006, Sol. Phys., 234, 379

Cauley, P. W., Johns-Krull, C. M., Hamilton, C. M., & Lockhart, K. 2012, ApJ, 756, 68

Chaboyer, B., Demarque, P., & Pinsonneault, M. H. 1995, ApJ, 441, 865

Chaplin, W. J., Sanchis-Ojeda, R., Campante, T. L., et al. 2013, arXiv:1302.3728

Charbonnel, C., Decressin, T., Amard, L., Palacios, A., & Talon, S. 2013, arXiv:1304.5470

Cieza, L., & Baliber, N. 2007, ApJ, 671, 605

Cohen, O., Drake, J. J., Kashyap, V. L., Sokolov, I. V., & Gombosi, T. I. 2010, ApJL, 723, L64

Collier Cameron, A., Campbell, C. G., & Quaintrell, H. 1995, A&A, 298, 133

Covey, K. R., Greene, T. P., Doppmann, G. W., & Lada, C. J. 2005, AJ, 129, 2765

Cranmer, S. R., & Saar, S. H. 2011, ApJ, 741, 54

Dahm, S. E., Slesnick, C. L., & White, R. J. 2012, ApJ, 745, 56

Deheuvels, S., García, R. A., Chaplin, W. J., et al. 2012, ApJ, 756, 19

Delfosse, X., Forveille, T., Perrier, C., & Mayor, M. 1998, A&A, 331, 581

Delorme, P., Collier Cameron, A., Hebb, L., et al. 2011, MNRAS, 413, 2218

Dobbs-Dixon, I., Lin, D. N. C., & Mardling, R. A. 2004, ApJ, 610, 464

Donati, J.-F., Semel, M., Carter, B. D., Rees, D. E., & Collier Cameron, A. 1997, MNRAS, 291, 658

Dravins, D., Lindegren, L., & Torkelsson, U. 1990, A&A, 237, 137

Dufton, P. L., Dunstall, P. R., Evans, C. J., et al. 2011, ApJL, 743, L22

Durney, B. R., & Latour, J. 1978, Geophysical and Astrophysical Fluid Dynamics, 9, 241

Edwards, S., Strom, S. E., Hartigan, P., et al. 1993, AJ, 106, 372

Eggenberger, P., Maeder, A., & Meynet, G. 2005, A&A, 440, L9

Eggenberger, P., Montalbán, J., & Miglio, A. 2012, A&A, 544, L4

Ekström, S., Meynet, G., Maeder, A., & Barblan, F. 2008, A&A, 478, 467

Ekström, S., Georgy, C., Eggenberger, P., et al. 2012, A&A, 537, A146

Epstein, C. R., & Pinsonneault, M. H. 2012, arXiv:1203.1618

Ferreira, J., Pelletier, G., & Appl, S. 2000, MNRAS, 312, 387

Gaigé, Y. 1993, A&A, 269, 267

Gallet, F., & Bouvier, J. 2013, arXiv:1306.2130

Gastine, T., Morin, J., Duarte, L., et al. 2013, A&A, 549, L5

Ghosh, P., Pethick, C. J., & Lamb, F. K. 1977, ApJ, 217, 578

Gizon, L., & Solanki, S. K. 2003, ApJ, 589, 1009

Goupil, M. J., Samadi, R., Lochard, J., Dziembowski, W. A., & Pamyatnykh, A. 2004, Stellar Structure and Habitable Planet Finding, 538, 133

Gray, D. F. 1973, ApJ, 184, 461

Gray, D. F. 1977, ApJ, 211, 198

Gregory, S. G., Donati, J.-F., Morin, J., et al. 2012, ApJ, 755, 97

Griffin, R. F. 1967, ApJ, 148, 465

Hartmann, L., & Stauffer, J. R. 1989, AJ, 97, 873

Hartmann, L., Hewett, R., Stahler, S., & Mathieu, R. D. 1986, ApJ, 309, 275

Hernández, J., Hartmann, L., Megeath, T., et al. 2007, ApJ, 662, 106

Herbst, W., Bailer-Jones, C. A. L., & Mundt, R. 2001, ApJL, 554, L197

Herbst, W., Eislöffel, J., Mundt, R., & Scholz, A. 2007, Protostars and Planets V, 297

Huang, W., & Gies, D. R. 2006, ApJ, 648, 580

Irwin, J., & Bouvier, J. 2009, IAU Symposium, 258, 363

Irwin, J., Aigrain, S., Bouvier, J., et al. 2009, MNRAS, 392, 1456

Irwin, J., Berta, Z. K., Burke, C. J., et al. 2011, ApJ, 727, 56

Irwin, J., Hodgkin, S., Aigrain, S., et al. 2008, MNRAS, 383, 1588

Kawaler, S. D. 1988, ApJ, 333, 236

Kervella, P., Thévenin, F., Di Folco, E., & Ségransan, D. 2004, A&A, 426, 297

Khokhlova, V. L. 1976, Astronomische Nachrichten, 297, 203

Königl, A. 1991, ApJL, 370, L39

Kraft, R. P. 1967, ApJ, 150, 551

Kraft, R. P. 1970, Spectroscopic Astrophysics. An Assessment of the Contributions of Otto Struve, 385

Krishnamurthi, A., Pinsonneault, M. H., Barnes, S., & Sofia, S. 1997, ApJ, 480, 303

Lagarde, N., Decressin, T., Charbonnel, C., et al. 2012, A&A, 543, A108

Lanza, A. F. 2010, A&A, 512, A77

Le Blanc, T. S., Covey, K. R., & Stassun, K. G. 2011, AJ, 142, 55

Le Bouquin, J.-B., Absil, O., Benisty, M., et al. 2009, A&A, 498, L41

Leroy, J. L., Bagnulo, S., Landolfi, M., & Landi Degl'Innocenti, E. 1994, A&A, 284, 174

MacGregor, K. B., & Brenner, M. 1991, ApJ, 376, 204

Marsden, S. C., Jardine, M. M., Ramírez Vélez, J. C., et al. 2011, MNRAS, 413, 1939

Matt, S., & Pudritz, R. E. 2008, ApJ, 681, 391

Matt, S. P., MacGregor, K. B., Pinsonneault, M. H., & Greene, T. P. 2012, ApJL, 754, L26

Mayor, M., Marmier, M., Lovis, C., et al. 2011, arXiv:1109.2497

McQuillan, A., Aigrain, S., & Mazeh, T. 2013, arXiv:1303.6787

Meibom, S., Barnes, S. A., Latham, D. W., et al. 2011, ApJL, 733, L9

Mestel, L. 1984, Cool Stars, Stellar Systems, and the Sun, 193, 49

Meynet, G., & Maeder, A. 2000, A&A, 361, 101

Mohanty, S., & Basri, G. 2003, ApJ, 583, 451

Mohanty, S., & Shu, F. H. 2008, ApJ, 687, 1323

Monnier, J. D., Zhao, M., Pedretti, E., et al. 2007, Science, 317, 342

Morin, J., Donati, J.-F., Petit, P., et al. 2010, MNRAS, 407, 2269

Mosser, B., Baudin, F., Lanza, A. F., et al. 2009, A&A, 506, 245

Mosser, B., Goupil, M. J., Belkacem, K., et al. 2012, A&A, 548, A10

Najita, J. R., Carr, J. S., Glassgold, A. E., & Valenti, J. A. 2007, Protostars and Planets V, 507

Pinto, R. F., Brun, A. S., Jouve, L., & Grappin, R. 2011, ApJ, 737, 72

Raghavan, D., McAlister, H. A., Henry, T. J., et al. 2010, ApJS, 190, 1

Randich, S. 2010, IAU Symposium, 268, 275

Rebull, L. M., Wolff, S. C., & Strom, S. E. 2004, AJ, 127, 1029

Rebull, L. M., Stauffer, J. R., Megeath, S. T., Hora, J. L., & Hartmann, L. 2006, ApJ, 646, 297

Reiners, A., & Basri, G. 2008, ApJ, 684, 1390

Reiners, A., & Mohanty, S. 2012, ApJ, 746, 43

Reiners, A., & Schmitt, J. H. M. M. 2002, A&A, 384, 155

Reiners, A., Basri, G., & Browning, M. 2009, ApJ, 692, 538

Rodríguez-Ledesma, M. V., Mundt, R., & Eislöffel, J. 2009, A&A, 502, 883

Rosen, A. L., Krumholz, M. R., & Ramirez-Ruiz, E. 2012, ApJ, 748, 97

Rucinski, S. M. 1988, AJ, 95, 1895

Schatzman, E. 1962, Annales d'Astrophysique, 25, 18

Scholz, A., & Eislöffel, J. 2004, A&A, 419, 249

Scholz, A., & Eislöffel, J. 2005, A&A, 429, 1007

Scholz, A., Irwin, J., Bouvier, J., et al. 2011, MNRAS, 413, 2595

Schou, J., Antia, H. M., Basu, S., et al. 1998, ApJ, 505, 390

Semel, M. 1989, A&A, 225, 456

Sills, A., Pinsonneault, M. H., & Terndrup, D. M. 2000, ApJ, 534, 335

Skumanich, A. 1972, ApJ, 171, 565

Spiegel, E. A., & Zahn, J.-P. 1992, A&A, 265, 106

Stauffer, J. R. 1987, Cool Stars, Stellar Systems and the Sun, 291, 182

Stauffer, J. R., & Hartmann, L. W. 1987, ApJ, 318, 337

Strom, S. E., Wolff, S. C., & Dror, D. H. A. 2005, AJ, 129, 809

Talon, S., & Charbonnel, C. 2008, A&A, 482, 597

Tonry, J., & Davis, M. 1979, AJ, 84, 1511

van Belle, G. T. 2012, A&ARv, 20, 51

Vidotto, A. A., Opher, M., Jatenco-Pereira, V., & Gombosi, T. I. 2009, ApJ, 699, 441

Vidotto, A. A., Jardine, M., Opher, M., Donati, J. F., & Gombosi, T. I. 2011, MNRAS, 412, 351

Vogel, S. N., & Kuhi, L. V. 1981, ApJ, 245, 960

Vogt, S. S., & Penrod, G. D. 1983, PASP, 95, 565

von Zeipel, H. 1924, MNRAS, 84, 665

Weber, E. J., & Davis, L., Jr. 1967, ApJ, 148, 217

Wolff, S. C., Strom, S. E., & Hillenbrand, L. A. 2004, ApJ, 601, 979

Wolff, S. C., Strom, S. E., Dror, D., & Venn, K. 2007, AJ, 133, 1092

Wright, J. T., Marcy, G. W., Howard, A. W., et al. 2012, ApJ, 753, 160

Wright, N. J., Drake, J. J., Mamajek, E. E., & Henry, G. W. 2011, ApJ, 743, 48

Zahn, J.-P. 1977, A&A, 57, 383

Zahn, J.-P., & Bouchet, L. 1989, A&A, 223, 112

Zanni, C., & Ferreira, J. 2013, A&A, 550, A99

Zorec, J., & Royer, F. 2012, A&A, 537, A120